


Latent Space Diffusion Models of Cryo-EM Structures

Karsten Kreis^{1,*} Tim Dockhorn^{1,2,3,*} Zihao Li⁴ Ellen Zhong⁴

¹NVIDIA ²University of Waterloo ³Vector Institute ⁴Princeton University
 kkreis@nvidia.com, tim.dockhorn@uwaterloo.ca, {z11665,zhonge}@princeton.edu

Abstract

Cryo-electron microscopy (cryo-EM) is unique among tools in structural biology in its ability to image large, dynamic protein complexes. Key to this ability is image processing algorithms for heterogeneous cryo-EM reconstruction, including recent deep learning-based approaches. The state-of-the-art method cryoDRGN uses a Variational Autoencoder (VAE) framework to learn a continuous distribution of protein structures from single particle cryo-EM imaging data. While cryoDRGN can model complex structural motions, the Gaussian prior distribution of the VAE fails to match the aggregate approximate posterior, which prevents generative sampling of structures especially for multi-modal distributions (e.g. compositional heterogeneity). Here, we train a diffusion model as an expressive, learnable prior in the cryoDRGN framework. Our approach learns a high-quality generative model over molecular conformations directly from cryo-EM imaging data. We show the ability to sample from the model on two synthetic and two real datasets, where samples accurately follow the data distribution unlike samples from the VAE prior distribution. We also demonstrate how the diffusion model prior can be leveraged for fast latent space traversal and interpolation between states of interest. By learning an accurate model of the data distribution, our method unlocks tools in generative modeling, sampling, and distribution analysis for heterogeneous cryo-EM ensembles.

1 Introduction

Single particle cryo-electron microscopy (cryo-EM) is a biological imaging modality capable of visualizing the 3D structure of large biomolecular complexes at (near-)atomic resolution [1]. In this technique, a thin layer of an aqueous sample of the molecule of interest is flash frozen and imaged with a transmission electron microscope. After initial pre-processing of the raw micrographs, the dataset consists of a set of noisy projection images, where each image \mathbf{x} contains a 2D projection of a molecular volume $V : \mathbb{R}^3 \rightarrow \mathbb{R}$ captured in an unknown *pose* $(R, t) \in SO(3) \times \mathbb{R}^2$ [2]. Since each image contains a unique molecule, to account for structural variation between the imaged molecules, reconstruction methods introduce a latent variable \mathbf{z} to define a *conformational space* $\mathcal{V}(\cdot, \mathbf{z}) : \mathbb{R}^3 \rightarrow \mathbb{R}$ from which volumes V are sampled. Thus, *heterogeneous cryo-EM reconstruction* amounts to solving the inverse problem of estimating \mathcal{V} , \mathbf{z} , and (R, t) from the experimental images \mathbf{x} . Traditionally, common approaches for heterogeneous reconstruction use a discrete model for \mathcal{V} (e.g. a mixture model in 3D classification [3–5]); however, deep generative models have recently been introduced that are designed to capture more complex, continuous distributions of protein conformations [6–10].

CryoDRGN [6] is a state-of-the-art method for heterogeneous reconstruction based on deep generative modeling. In cryoDRGN, a neural field representation of the volume is conditioned on a generic,

*Equal contribution.

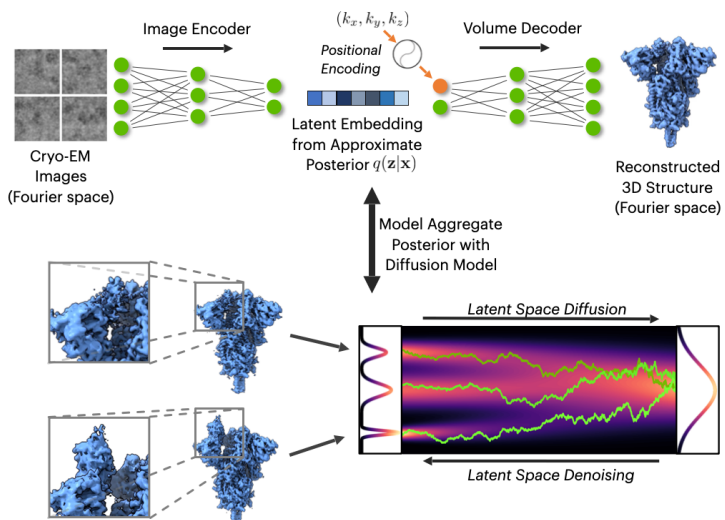


Figure 1: We first train cryoDRGN with a standard VAE objective (*top*). Then, we train a diffusion model in its latent space on the embedding distribution (*bottom*). The diffusion model learns a representation of the conformational space of the molecule. Generating different latents \mathbf{z} corresponds to sampling different molecular configurations (e.g., the blue SARS-CoV-2 spike protein is sampled in receptor binding domain open vs. closed states). (Dataset: Walls et al. [25])

continuous latent variable $\mathbf{z} \in \mathbb{R}^{\dim(\mathbf{z})}$ describing the molecule’s conformational space \mathcal{V} . CryoDRGN uses a standard Variational Autoencoder (VAE) [11, 12] framework for amortized inference of \mathbf{z} and reconstruction of V . However, the standard Gaussian prior that is employed in regular VAEs to model the latent space distribution cannot accurately match the aggregate posterior distribution (known as the *prior hole problem* [13–21]). The latter can be a complex, multi-modal distribution, in particular for molecules with complex topologies and conformational state spaces. Because of this, cryoDRGN is only used as an efficient reconstruction method, but not as a generative model that can synthesize meaningful latents from its prior and generate plausible volumes V .

Recently, Vahdat et al. [13] leveraged expressive denoising diffusion generative models [22–24] to better capture complex aggregate posteriors in VAEs for RGB image modeling tasks. In this work, we propose to leverage a similar latent diffusion model framework in cryoDRGN, and we train a diffusion prior that can effectively encode the conformational states of the molecules (see Fig. 1). In experiments on synthetic and real datasets, we verify that our latent diffusion model indeed accurately captures the latent embedding distribution. Moreover, we show how we can leverage the model for accelerated iterative sampling and traversal in latent space as well as for interpolations between different states, thereby effectively simulating conformational transitions. Our approach learns a true generative model of the conformational space directly from cryo-EM imaging data. We envision that our framework paves the way towards several technical extensions and novel applications in protein structure modeling with cryo-EM data.

2 Methods

CryoDRGN [6, 26] is designed as a VAE with an MLP encoder neural network that consumes Fourier-space cryo-EM images \mathbf{x} and parametrizes a diagonal Gaussian approximate posterior $q_\phi(\mathbf{z}|\mathbf{x})$ over latent variables \mathbf{z} . CryoDRGN’s probabilistic Gaussian decoder $p_\phi(\mathbf{x}|\mathbf{z})$ is parametrized as a neural field [27], also based on an MLP, taking both latent variables \mathbf{z} and Fourier space coordinates $\mathbf{k} = (k_x, k_y, k_z)$ (processed through sinusoidal positional encodings [6, 28]) as inputs. The field outputs the Coulomb scattering potential in Fourier space at \mathbf{k} . By the image formation model, 2D central slices of the 3D densities in Fourier space correspond to the input cryo-EM images; During training, a 2D grid of oriented \mathbf{k} are rendered to form a reconstruction loss. However, this requires knowledge of the pose of the molecule, as discussed in Sec. 1. Therefore, cryoDRGN also incorporates an image pose inference step [7]. Specifically, a global search over rotations and translations is performed to find the maximum likelihood pose under the decoder distribution, given the inferred latent variable \mathbf{z} . Finally, cryoDRGN is trained with a modified variational lower bound [11, 12] (we omit indicating pose inference here for brevity):

$$\arg \max_{\phi} \mathbb{E}_{\mathbf{x} \sim p_{\text{data}}(\mathbf{x})} \mathbb{E}_{\mathbf{z} \sim q_{\phi}(\mathbf{z}|\mathbf{x})} [\log p_{\phi}(\mathbf{x}|\mathbf{z})] - \beta \text{KL}(q_{\phi}(\mathbf{z}|\mathbf{x})||p(\mathbf{z})), \quad (1)$$

with standard Gaussian prior $p(\mathbf{z}) \sim \mathcal{N}(\mathbf{0}, \mathbf{I})$. The Kullback Leibler (KL) divergence weighting is chosen to be $\beta = 1/\dim(\mathbf{z}) < 1$ in cryoDRGN. This effectively reduces the KL regularization and gives more flexibility to the model to learn diverse encodings that translate to accurate reconstructions (however, it also encourages a mismatch between prior and aggregate approximate posterior; see

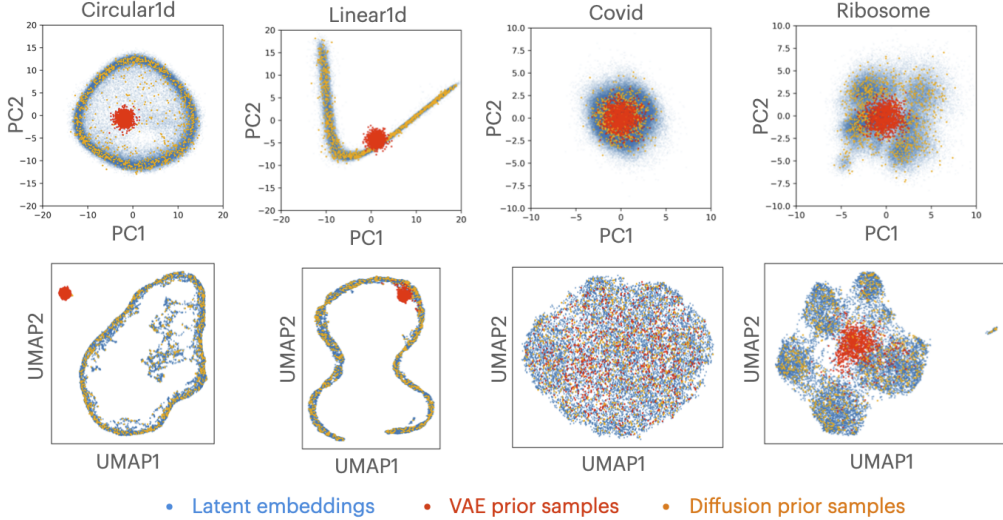


Figure 2: Training a diffusion model on cryoDRGN embeddings accurately models the data distribution. CryoDRGN latent embeddings are shown in blue. 1,000 samples from the diffusion model prior or VAE prior are shown in orange or red, respectively. The latent space is visualized in 2D either by projecting samples along the first two principal components of the latent embeddings (*top row*) or with Uniform Manifold Approximation and Projection (UMAP) [41] (*bottom row*). Also see Fig. 7.

discussion below). By sampling the entire neural field via \mathbf{k} , cryoDRGN can reconstruct 3D cryo-EM density volumes V , given a latent variable \mathbf{z} .

Diffusion Models [22–24] are a novel class of deep generative models that has recently demonstrated state-of-the-art quality in image synthesis [29–38] as well as many other applications. In this work, we use continuous-time diffusion models [23] and follow Karras et al. [39]. Let $p(\mathbf{x}; \sigma)$ denote the distribution obtained by adding i.i.d. σ^2 -variance Gaussian noise to the data distribution $p_{\text{data}}(\mathbf{x})$. For sufficiently large σ_{max} , $p(\mathbf{x}; \sigma_{\text{max}}^2)$ is almost indistinguishable from σ_{max}^2 -variance Gaussian noise. Based on this observation, diffusion models sample high variance Gaussian noise $\mathbf{x}_0 \sim \mathcal{N}(\mathbf{0}, \sigma_{\text{max}}^2)$ and sequentially denoise \mathbf{x}_0 into $\mathbf{x}_i \sim p(\mathbf{x}_i; \sigma_i)$, $i \in [0, \dots, M]$, with $\sigma_i < \sigma_{i-1}$ ($\sigma_0 = \sigma_{\text{max}}$). If $\sigma_M = 0$, then \mathbf{x}_0 is distributed according to the data. In practice, the sequential denoising is often implemented through the numerical simulation of the *Probability Flow* ordinary differential equation (ODE) [23]

$$d\mathbf{x} = -\dot{\sigma}(t)\sigma(t)\nabla_{\mathbf{x}} \log p(\mathbf{x}; \sigma(t)) dt, \quad (2)$$

where $\nabla_{\mathbf{x}} \log p(\mathbf{x}; \sigma)$ is the *score function* [40]. The schedule $\sigma(t) : [0, 1] \rightarrow \mathbb{R}_+$ is user-specified and $\dot{\sigma}(t)$ denotes the time derivative of $\sigma(t)$. Alternatively, we may also use a stochastic differential equation (SDE) [23, 39] that effectively samples the same distribution (see App. A.1). Diffusion model training reduces to learning the score model s_{θ} . The model can, for example, be parameterized as $\nabla_{\mathbf{x}} \log p(\mathbf{x}; \sigma) \approx s_{\theta} = (D_{\theta}(\mathbf{x}; \sigma) - \mathbf{x})/\sigma^2$ [39], where D_{θ} is a learnable *denoiser* that, given a noisy data point $\mathbf{x} + \mathbf{n}$, $\mathbf{x} \sim p_{\text{data}}(\mathbf{x})$, $\mathbf{n} \sim \mathcal{N}(\mathbf{0}, \sigma^2)$ and conditioned on the noise level σ , tries to predict the clean \mathbf{x} . The denoiser D_{θ} can be trained by minimizing an L_2 -loss ($\lambda(\sigma) : \mathbb{R}_+ \rightarrow \mathbb{R}_+$ is a weighting function)

$$\arg \min_{\theta} \mathbb{E}_{\mathbf{x} \sim p_{\text{data}}(\mathbf{x}), \sigma \sim p(\sigma), \mathbf{n} \sim \mathcal{N}(\mathbf{0}, \sigma^2)} [\lambda(\sigma) \|D_{\theta}(\mathbf{x} + \mathbf{n}, \sigma) - \mathbf{x}\|_2^2]. \quad (3)$$

Latent Space Diffusion Models in cryoDRGN. Since cryoDRGN is trained in regular VAE-fashion with a standard Gaussian prior, it can suffer from the prior hole problem [13–21], i.e., a mismatch between the aggregate approximate posterior and prior distributions. As we show in Sec. 3.2, samples drawn from the Gaussian prior fail to reproduce the latent embedding distribution. This implies that, although cryoDRGN is a state-of-the-art cryo-EM reconstruction approach, we cannot use it as a generative model and sample latents \mathbf{z} according to the modeled distribution of conformational states. Furthermore, prior samples will not necessarily decode into coherent cryo-EM density volumes.

Inspired by recent works on RGB image synthesis that fit diffusion models in the latent space of VAEs [13, 19, 31], we propose to model cryoDRGN’s latent embedding distribution with an expressive

diffusion model. We can formulate the training objective of our latent space diffusion model as

$$\arg \min_{\theta} \mathbb{E}_{\mathbf{x} \sim p_{\text{data}}(\mathbf{x}), \mathbf{z} \sim q_{\phi}(\mathbf{z}|\mathbf{x}), \sigma \sim p(\sigma), \mathbf{n} \sim \mathcal{N}(\mathbf{0}, \sigma^2)} [\lambda(\sigma) \|D_{\theta}(\mathbf{z} + \mathbf{n}, \sigma) - \mathbf{z}\|_2^2], \quad (4)$$

where we extract latent embeddings \mathbf{z} from the cryo-EM images \mathbf{x} with cryoDRGN’s encoder $q_{\phi}(\mathbf{z}|\mathbf{x})$ and fit the diffusion model to the latent space distribution formed by the latent variables \mathbf{z} . Note that we are training in a two-stage manner: We first train a cryoDRGN VAE model (with the objective in Eq. (1)), which we then freeze. Next, we train the diffusion model in latent space with the objective in Eq. (4). Sampling from the diffusion model and feeding the synthesized latent variables to cryoDRGN’s neural field decoder allows us to sample conformational states of the modeled protein. Our approach is visualized in Fig. 1. All training details are provided in App. A.1.

3 Results

3.1 Datasets

We run experiments on cryoDRGN models trained on a total of four datasets: 2 synthetic datasets, "linear1d" and "circular1d", where ground truth volumes are generated along a continuous 1-dimensional linear or circular reaction coordinate, respectively [6]; "ribosome", a real dataset containing a mixture of assembly intermediates of the *E. coli* large ribosomal subunit from EMPIAR-10076 [42], and "covid", a real dataset of the SARS-CoV-2 spike protein transitioning between the receptor binding domain (RBD) open and closed conformations [25]. CryoDRGN models were trained with either an 8 or 10 dimensional latent variable model. The sizes of these datasets range from 50k to 277k cryo-EM images. Additional dataset and cryoDRGN training details are provided in App. A.1.

3.2 Generative Model Sampling

We train a diffusion model on latent encodings from cryoDRGN to model the aggregate approximate posterior distribution for several datasets exhibiting different types of heterogeneity.

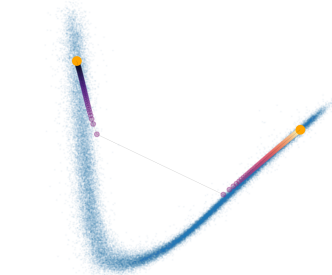


Figure 4: Conformational state interpolation with the diffusion model prior for linear1d; Also see Fig. 8.

Once trained, we sample 1,000 latent variables \mathbf{z} from the diffusion model (sampling details in App. A.1). A visualization of these samples, together with embeddings of the data distribution and VAE prior samples, is shown in Fig. 2. While the diffusion model accurately models the data, samples from the original Gaussian VAE prior fail to model the data distribution; the mismatch is worst for highly structured latent spaces. In Tab. 1, we also show quantitatively that the diffusion model prior captures the distribution of the data’s latent encodings much more accurately than the standard Gaussian prior. Furthermore, in Fig. 3 we visualize corresponding 3D volumes for circular1d. We find that while the diffusion model samples decode into realistic molecular conformations, the VAE prior samples, which are located in an empty region of the latent space, produce incorrect volumes with artifacts in the heterogeneous region. Our experiments verify that the learned diffusion model prior is able to accurately model the latent embedding distribution.

Table 1: Total Variation Distance in PC1 marginal space between data embedding distribution and diffusion prior as well as Gaussian VAE prior distributions.

Dataset	Latent Diffusion Model Prior	Standard Gaussian VAE Prior
circular1d	0.015	0.82
linear1d	0.015	0.86
covid	0.005	0.19
ribosome	0.015	0.58

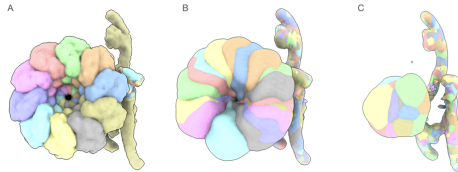


Figure 3: circular1d volumes viewed as isosurface contour. **A:** Ground truth volumes. **B:** 20 volumes sampled from diffusion model prior. **C:** 20 volumes sampled from standard Gaussian VAE prior.

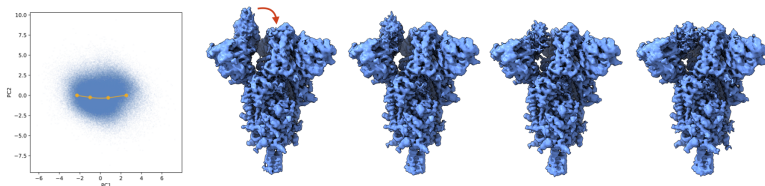


Figure 5: Diffusion model-based interpolation in latent space (*left*) between open and closed conformational states of the SARS-CoV-2 spike protein (visualized on the *right*).

3.3 Diffusion Model Interpolations

We may be interested in modeling transitions between structures by interpolating between their corresponding encodings in latent space. However, as discussed, the latent space distribution can be complex and multi-modal and a linear interpolation directly in latent space between different encodings may pass through prior holes, i.e., “empty” regions in latent space, which may produce artifacts. However, our diffusion model effectively maps all states into its own Gaussian prior distribution ($\mathbf{x}_0 \sim \mathcal{N}(\mathbf{0}, \sigma_{\max}^2)$, see Sec. 2), and interpolating within this Gaussian space is, in fact, valid. In particular, there are no prior holes in this space, because the diffusion model’s forward diffusion process converges to this distribution by construction. Using the deterministic Probability Flow ODE (Eq. (2)), we encode states \mathbf{z}_A and \mathbf{z}_B in the diffusion model’s own prior (see App. A.1 for details). Denoting the resulting encodings as $\hat{\mathbf{z}}_A$ and $\hat{\mathbf{z}}_B$, respectively, we then linearly interpolate $\hat{\mathbf{z}}_{AB}(y) = (1 - y)\hat{\mathbf{z}}_A + y\hat{\mathbf{z}}_B$, where $y \in [0, 1]$ is an interpolation parameter (more sophisticated interpolations, such as spherical, are possible, but we did not observe any benefits). Again using the Probability Flow ODE, we decode states $\hat{\mathbf{z}}_{AB}(y)$ along the interpolation back to $\mathbf{z}_{AB}(y)$ in cryoDRGN’s original latent space.

In Fig. 5, we visualize such an interpolation trajectory between the open and closed conformations of the SARS-CoV-2 spike protein and we observe a smooth transition. We use cryoDRGN’s decoder to generate corresponding molecular volumes. We also show the latent space trajectory for an interpolation between two far-apart states in *linear1d*, a challenging case due to its highly structured latent space (Fig. 4). We performed equidistant steps in the diffusion model’s Gaussian prior and observe a “jump” behavior. This is expected, as it merely implies that the diffusion model has learned a sharp transition in its Probability Flow ODE. Importantly, no samples are generated in the empty region during the jump.

3.4 Efficient Latent Space Traversal and Sampling

The diffusion model’s Probability Flow ODE can be interpreted as an instance of a continuous Normalizing Flow [43, 44]. Previous work has leveraged Normalizing Flows [45] and other invertible mappings [46] to accelerate Markov Chain Monte Carlo (MCMC) algorithms such as Hamiltonian Monte Carlo and Langevin dynamics [47]: The MCMC chain is run in the Gaussian prior of the invertible mapping, where no barriers are present, while the Flow non-linearly transforms the samples along the sampling path such that they effectively jump between states and efficiently traverse the complex distribution of interest at the output of the Flow (cryoDRGN’s latent space distribution in our case). In Fig. 6, we demonstrate that running Langevin dynamics in the Gaussian prior space of our latent diffusion model allows us to very efficiently traverse the molecular manifold, making large jumps between distant states. Note that sampling with an iterative sampler like Langevin dynamics can be advantageous, because it would allow us to trivially incorporate additional potential energy terms, which can be more difficult in regular diffusion model sampling.

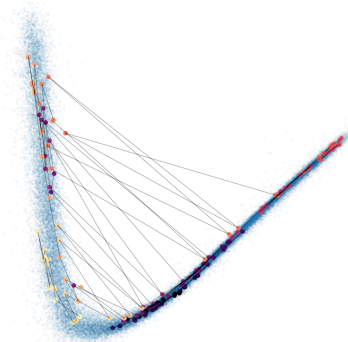


Figure 6: Langevin dynamics sampling in the diffusion model prior results in fast exploration of the latent molecular manifold (*linear1d*; also see Fig. 9).

4 Future Directions

We have shown that a diffusion model incorporated in cryoDRGN’s latent space has learned an accurate representation of the conformational state space of the imaged proteins, directly from cryo-EM imaging data. We envision that we can leverage this as a promising tool for relevant and novel

applications in generative modeling, accelerated sampling, and distribution analysis in cryo-EM and molecular modeling.

Conditional Generative Modeling. We have demonstrated that random samples from the diffusion model accurately reproduce the molecular manifold. But one may also be able to perform conditional generation: For instance, we envision applications where molecular conformations are sampled from the latent diffusion model based on guidance from auxiliary scoring algorithms or classifiers to fulfill certain properties, like high binding affinity to a ligand. Methodologically, one could build on classifier- and classifier-free guidance techniques from the literature on diffusion models [23, 30, 48]. Moreover, since we have learned a smooth continuous latent manifold of the data that we can traverse easily, as we demonstrated, we can also employ gradient-based optimization techniques in latent space to optimize the corresponding conformational states according to different criteria [49].

Coupling with Atomic Models. Future versions of cryoDRGN might perform direct atomic model reconstruction, a direction also explored by Zhong et al. [8], Rosenbaum et al. [50]. In general, directly inferring an accurate atomic model from cryo-EM imaging data is an extraordinarily challenging problem without any additional inductive biases or priors. However, recently diffusion models have also been used for atomic small molecule and protein generation [51–59]. Such models can potentially serve as powerful priors for cryo-EM-based atomic protein structure prediction. Combined with an appropriate decoder neural network that operates in atom coordinates, our latent diffusion model would then effectively be a generative model not only over 3D density volumes, but also their underlying atomic structures.

Molecular Simulation. Here, we demonstrated that we can interpolate between different protein states and efficiently traverse the latent space using diffusion model-enhanced MCMC techniques. In fact, MCMC methods like Langevin dynamics are widely used in statistical mechanics and molecular dynamics [60, 61] to sample molecular conformations. When combined with atomic coordinate outputs, future work could explore leveraging our latent diffusion model for accelerated molecular dynamics simulations as well as for free energy calculations between relevant protein states.

End-to-end Training and Hierarchical Models. There are also promising technical extensions: For instance, end-to-end training of cryoDRGN together with the latent diffusion model, similarly to Vahdat et al. [13], may allow cryoDRGN to learn better embeddings and perform better reconstruction by offering more flexibility to cryoDRGN in how to distribute encodings in latent space. Moreover, deep hierarchical VAEs are often used to improve model expressivity in RGB image synthesis tasks [17, 62]. CryoDRGN would likely benefit from similar hierarchical architectures. Such models can sometimes even learn a semantic disentanglement of different features of the data [63]—exploring this in the context of protein structure modeling would be highly interesting. For instance, we might learn one diffusion model that captures the main data clusters, i.e., main conformational states, and another one to model intra-cluster variation. These directions will be particularly relevant when modeling large-scale, complex and heterogeneous protein data.

In conclusion, we believe that combining state-of-the-art cryo-EM reconstruction methods such as cryoDRGN with modern deep generative learning approaches such as diffusion models has the potential to lead to powerful new tools and promising applications both in cryo-EM reconstruction and in biomolecular modeling more generally.

References

- [1] Y Cheng. Single-particle cryo-EM—how did it get here and where will it go. *Science*, 361, 2018.
- [2] Amit Singer and Fred J Sigworth. Computational methods for Single-Particle electron cryomicroscopy. *Annu Rev Biomed Data Sci*, 3:163–190, July 2020.
- [3] Sjors H W Scheres. Chapter eleven - classification of structural heterogeneity by Maximum-Likelihood methods. In Grant J Jensen, editor, *Methods in Enzymology*, volume 482, pages 295–320. Academic Press, January 2010.
- [4] D Lyumkis, A F Brilot, D L Theobald, and N Grigorieff. Likelihood-based classification of cryo-EM images using FREALIGN. *J. Struct. Biol.*, 183, 2013.

- [5] A Punjani, J L Rubinstein, D J Fleet, and M Brubaker. cryoSPARC: algorithms for rapid unsupervised cryo-EM structure determination. *Nat. Methods*, 14, 2017.
- [6] Ellen D. Zhong, Tristan Bepler, Joseph H. Davis, and Bonnie Berger. Reconstructing continuous distributions of 3d protein structure from cryo-em images. In *International Conference on Learning Representations*, 2020.
- [7] Ellen D Zhong, Adam Lerer, Joseph H Davis, and Bonnie Berger. CryoDRGN2: Ab initio neural reconstruction of 3D protein structures from real cryo-EM images. In *Proceedings of the IEEE/CVF International Conference on Computer Vision*, pages 4066–4075, 2021.
- [8] Ellen D Zhong, Adam Lerer, Joseph H Davis, and Bonnie Berger. Exploring generative atomic models in cryo-EM reconstruction. July 2021.
- [9] A Punjani and D J Fleet. 3D flexible refinement: Structure and motion of flexible proteins from Cryo-EM. *bioRxiv*, 2021.
- [10] Claire Donnat, Axel Levy, Frederic Poitevin, Ellen Zhong, and Nina Miolane. Deep generative modeling for volume reconstruction in Cryo-Electron microscopy. January 2022.
- [11] Diederik P Kingma and Max Welling. Auto-encoding variational bayes. In *The International Conference on Learning Representations (ICLR)*, 2014.
- [12] Danilo Jimenez Rezende, Shakir Mohamed, and Daan Wierstra. Stochastic backpropagation and approximate inference in deep generative models. In *International Conference on Machine Learning*, pages 1278–1286, 2014.
- [13] Arash Vahdat, Karsten Kreis, and Jan Kautz. Score-based Generative Modeling in Latent Space. In *Neural Information Processing Systems (NeurIPS)*, 2021.
- [14] Jakub Tomczak and Max Welling. Vae with a vampprior. In *International Conference on Artificial Intelligence and Statistics*, pages 1214–1223, 2018.
- [15] Hiroshi Takahashi, Tomoharu Iwata, Yuki Yamanaka, Masanori Yamada, and Satoshi Yagi. Variational autoencoder with implicit optimal priors. *Proceedings of the AAAI Conference on Artificial Intelligence*, 33(01):5066–5073, Jul. 2019.
- [16] Matthias Bauer and Andriy Mnih. Resampled priors for variational autoencoders. In Kamalika Chaudhuri and Masashi Sugiyama, editors, *Proceedings of the Twenty-Second International Conference on Artificial Intelligence and Statistics*, volume 89 of *Proceedings of Machine Learning Research*, pages 66–75. PMLR, 16–18 Apr 2019.
- [17] Arash Vahdat and Jan Kautz. NVAE: A Deep Hierarchical Variational Autoencoder. In *Neural Information Processing Systems (NeurIPS)*, 2020.
- [18] Jyoti Aneja, Alexander Schwing, Jan Kautz, and Arash Vahdat. NCP-VAE: Variational autoencoders with noise contrastive priors. In *Advances in Neural Information Processing Systems*, 2021.
- [19] Abhishek Sinha, Jiaming Song, Chenlin Meng, and Stefano Ermon. D2C: Diffusion-Denoising Models for Few-shot Conditional Generation. *arXiv:2106.06819*, 2021.
- [20] Mihaela Rosca, Balaji Lakshminarayanan, and Shakir Mohamed. Distribution matching in variational inference. *arXiv preprint arXiv:1802.06847*, 2018.
- [21] Matthew D Hoffman and Matthew J Johnson. Elbo surgery: yet another way to carve up the variational evidence lower bound. In *Workshop in Advances in Approximate Bayesian Inference, NeurIPS*, 2016.
- [22] Jascha Sohl-Dickstein, Eric Weiss, Niru Maheswaranathan, and Surya Ganguli. Deep Unsupervised Learning using Nonequilibrium Thermodynamics. In *International Conference on Machine Learning*, 2015.

- [23] Yang Song, Jascha Sohl-Dickstein, Diederik P Kingma, Abhishek Kumar, Stefano Ermon, and Ben Poole. Score-Based Generative Modeling through Stochastic Differential Equations. In *International Conference on Learning Representations*, 2021.
- [24] Jonathan Ho, Ajay Jain, and Pieter Abbeel. Denoising Diffusion Probabilistic Models. In *Advances in Neural Information Processing Systems*, 2020.
- [25] Alexandra C Walls, Young-Jun Park, M Alejandra Tortorici, Abigail Wall, Andrew T McGuire, and David Veessler. Structure, function, and antigenicity of the SARS-CoV-2 spike glycoprotein. *Cell*, 181(2):281–292.e6, apr 2020.
- [26] Ellen D Zhong, Tristan Bepler, Bonnie Berger, and Joseph H Davis. CryoDRGN: reconstruction of heterogeneous cryo-EM structures using neural networks. *Nat. Methods*, 18(2):176–185, February 2021.
- [27] Yiheng Xie, Towaki Takikawa, Shunsuke Saito, Or Litany, Shiqin Yan, Numair Khan, Federico Tombari, James Tompkin, Vincent Sitzmann, and Srinath Sridhar. Neural fields in visual computing and beyond. November 2021.
- [28] Ben Mildenhall, Pratul P. Srinivasan, Matthew Tancik, Jonathan T. Barron, Ravi Ramamoorthi, and Ren Ng. Nerf: Representing scenes as neural radiance fields for view synthesis. In *ECCV*, 2020.
- [29] Alexander Quinn Nichol and Prafulla Dhariwal. Improved Denoising Diffusion Probabilistic Models. In *International Conference on Machine Learning*, 2021.
- [30] Prafulla Dhariwal and Alex Nichol. Diffusion Models Beat GANs on Image Synthesis. In *Neural Information Processing Systems*, 2021.
- [31] Robin Rombach, Andreas Blattmann, Dominik Lorenz, Patrick Esser, and Björn Ommer. High-Resolution Image Synthesis with Latent Diffusion Models. *arXiv:2112.10752*, 2021.
- [32] Chitwan Saharia, Jonathan Ho, William Chan, Tim Salimans, David J Fleet, and Mohammad Norouzi. Image Super-Resolution via Iterative Refinement. *arXiv:2104.07636*, 2021.
- [33] Chitwan Saharia, William Chan, Huiwen Chang, Chris A. Lee, Jonathan Ho, Tim Salimans, David J. Fleet, and Mohammad Norouzi. Palette: Image-to-Image Diffusion Models. *arXiv:2111.05826*, 2021.
- [34] Kushagra Pandey, Avideep Mukherjee, Piyush Rai, and Abhishek Kumar. DiffuseVAE: Efficient, Controllable and High-Fidelity Generation from Low-Dimensional Latents. *arXiv:2201.00308*, 2022.
- [35] Tim Dockhorn, Arash Vahdat, and Karsten Kreis. Score-Based Generative Modeling with Critically-Damped Langevin Diffusion. In *International Conference on Learning Representations*, 2022.
- [36] Zhisheng Xiao, Karsten Kreis, and Arash Vahdat. Tackling the Generative Learning Trilemma with Denoising Diffusion GANs. In *International Conference on Learning Representations*, 2022.
- [37] Chitwan Saharia, William Chan, Saurabh Saxena, Lala Li, Jay Whang, Emily Denton, Seyed Kamyar Seyed Ghasemipour, Burcu Karagol Ayan, S Sara Mahdavi, Rapha Gontijo Lopes, et al. Photorealistic Text-to-Image Diffusion Models with Deep Language Understanding. *arXiv:2205.11487*, 2022.
- [38] Aditya Ramesh, Prafulla Dhariwal, Alex Nichol, Casey Chu, and Mark Chen. Hierarchical Text-Conditional Image Generation with CLIP Latents. *arXiv:2204.06125*, 2022.
- [39] Tero Karras, Miika Aittala, Timo Aila, and Samuli Laine. Elucidating the Design Space of Diffusion-Based Generative Models. *arXiv:2206.00364*, 2022.
- [40] Aapo Hyvärinen. Estimation of Non-Normalized Statistical Models by Score Matching. *Journal of Machine Learning Research*, 6:695–709, 2005. ISSN 1532-4435.

- [41] Leland McInnes, John Healy, and James Melville. UMAP: Uniform manifold approximation and projection for dimension reduction. February 2018.
- [42] J H Davis. Modular assembly of the bacterial large ribosomal subunit. *Cell*, 167, 2016.
- [43] Ricky T. Q. Chen, Yulia Rubanova, Jesse Bettencourt, and David Duvenaud. Neural Ordinary Differential Equations. *Advances in Neural Information Processing Systems*, 2018.
- [44] Will Grathwohl, Ricky T. Q. Chen, Jesse Bettencourt, Ilya Sutskever, and David Duvenaud. FFJORD: Free-form Continuous Dynamics for Scalable Reversible Generative Models. *International Conference on Learning Representations*, 2019.
- [45] Matthew Hoffman, Pavel Sountsov, Joshua V. Dillon, Ian Langmore, Dustin Tran, and Srinivas Vasudevan. Neutra-lizing bad geometry in hamiltonian monte carlo using neural transport. *arXiv:1903.03704*, 2019.
- [46] Zhisheng Xiao, Karsten Kreis, Jan Kautz, and Arash Vahdat. VAEBM: A Symbiosis between Variational Autoencoders and Energy-based Models. In *International Conference on Learning Representations*, 2021.
- [47] Radford M. Neal. MCMC Using Hamiltonian Dynamics. *Handbook of Markov Chain Monte Carlo*, 54:113–162, 2011.
- [48] Jonathan Ho and Tim Salimans. Classifier-Free Diffusion Guidance. In *NeurIPS 2021 Workshop on Deep Generative Models and Downstream Applications*, 2021.
- [49] Zaccary Alperstein, Artem Cherkasov, and Jason Tyler Rolfe. All smiles variational autoencoder. *arXiv preprint arXiv:1905.13343*, 2019.
- [50] Dan Rosenbaum, Marta Garnelo, Michal Zielinski, Charlie Beattie, Ellen Clancy, Andrea Huber, Pushmeet Kohli, Andrew W. Senior, John Jumper, Carl Doersch, S. M. Ali Eslami, Olaf Ronneberger, and Jonas Adler. Inferring a continuous distribution of atom coordinates from cryo-em images using vaes. *arXiv preprint arXiv:2106.14108*, 2021.
- [51] Chence Shi, Shitong Luo, Minkai Xu, and Jian Tang. Learning gradient fields for molecular conformation generation. In *International Conference on Machine Learning*, 2021.
- [52] Minkai Xu, Lantao Yu, Yang Song, Chence Shi, Stefano Ermon, and Jian Tang. GeoDiff: A Geometric Diffusion Model for Molecular Conformation Generation. In *International Conference on Learning Representations*, 2022.
- [53] Jaehyeong Jo, Seul Lee, and Sung Ju Hwang. Score-based Generative Modeling of Graphs via the System of Stochastic Differential Equations. *arXiv:2202.02514*, 2022.
- [54] Fang Wu, Qiang Zhang, Xurui Jin, Yinghui Jiang, and Stan Z. Li. A score-based geometric model for molecular dynamics simulations. *arXiv preprint arXiv:2204.08672*, 2022.
- [55] Bowen Jing, Gabriele Corso, Jeffrey Chang, Regina Barzilay, and Tommi Jaakkola. Torsional diffusion for molecular conformer generation. *arXiv preprint arXiv:2206.01729*, 2022.
- [56] Brian L. Trippe, Jason Yim, Doug Tischer, David Baker, Tamara Broderick, Regina Barzilay, and Tommi Jaakkola. Diffusion probabilistic modeling of protein backbones in 3d for the motif-scaffolding problem. *arXiv preprint arXiv:2206.04119*, 2022.
- [57] Emiel Hooeboom, Victor Garcia Satorras, Clément Vignac, and Max Welling. Equivariant diffusion for molecule generation in 3d. In *International Conference on Machine Learning (ICML)*, 2022.
- [58] Namrata Anand and Tudor Achim. Protein structure and sequence generation with equivariant denoising diffusion probabilistic models. *arXiv preprint arXiv:2205.15019*, 2022.
- [59] Lemeng Wu, Chengyue Gong, Xingchao Liu, Mao Ye, and Qiang Liu. Diffusion-based molecule generation with informative prior bridges. *arXiv preprint arXiv:2209.00865*, 2022.

- [60] Mark E. Tuckerman. *Statistical Mechanics: Theory and Molecular Simulation*. Oxford University Press, New York, 2010.
- [61] Benedict Leimkuhler and Charles Matthews. *Molecular Dynamics: With Deterministic and Stochastic Numerical Methods*. Interdisciplinary Applied Mathematics. Springer, 2015.
- [62] Rewon Child. Very deep {vae}s generalize autoregressive models and can outperform them on images. In *International Conference on Learning Representations*, 2021.
- [63] Konpat Preechakul, Nattanat Chatthee, Suttisak Wizadwongsa, and Supasorn Suwajanakorn. Diffusion Autoencoders: Toward a Meaningful and Decodable Representation. *arXiv:2111.15640*, 2021.
- [64] Ellen D. Zhong, Tristan Bepler, Bonnie Berger, and Joseph H. Davis. Data for "CryoDRGN: Reconstruction of heterogeneous cryo-EM structures using neural networks", January 2021. URL <https://doi.org/10.5281/zenodo.4355284>.
- [65] J. R. Dormand and P. J. Prince. A family of embedded Runge–Kutta formulae. *Journal of Computational and Applied Mathematics*, 6(1):19–26, 1980.
- [66] Peter E. Kloeden and Eckhard Platen. *Numerical Solution of Stochastic Differential Equations*. Springer, Berlin, 1992.

A Appendix

A.1 Implementation and Training Details

CryoDRGN. All cryoDRGN models are trained as in Zhong et al. [26]. Dataset and training details summarized in Table 2. Synthetic datasets are generated from atomic models as described in Zhong et al. [6] and with poses sampled uniformly from $SO(3)$ for rotations and $[-10, 10]^2$ pixels for translations. CryoDRGN models for *linear1d* and *circular1d* used positional encodings with geometrically spaced wavelengths between 1 and the Nyquist frequency and leaky ReLU activations. The cryoDRGN model for *ribosome* was downloaded from Zenodo [64]. All other settings unless otherwise specified were at their default values for cryoDRGN software version 1.0.

Table 2: Summary of the synthetic and experimental datasets and cryoDRGN training details. D is the resolution of the images, in pixels. N is the dataset size. Architecture is denoted as the width \times depth of the encoder and decoder MLPs.

Dataset	D	N	$\text{\AA}/\text{pix.}$	$ z $	Architecture	Epochs
<i>Linear1d</i>	128	50k	6	8	256×3	25
<i>Circular1d</i>	128	100k	6	8	256×3	25
<i>Ribosome</i> (EMPIAR-10076)[42]	256	87,328	1.6375	10	1024×3	50
<i>Covid</i> (Walls et al. [25])	256	276,549	1.640625	8	1024×3	25

Diffusion Model. Our latent space diffusion models follow the framework proposed in Karras et al. [39]. We set σ_{data} to the standard deviation of the training dataset. Our model parametrization, including the loss weighting $\lambda(\sigma)$, follows their setup (see column 4 in Table 2 in Karras et al. [39]). The neural network backbone of our diffusion models consists of a simple ResNet architecture with 16 hidden layers, using 128 hidden dimensions per layer. We train all models using Adam with a learning rate $3 \cdot 10^{-4}$ and batch size 1024. We set the EMA rate to 0.999.

Diffusion Model Sampling. For deterministic sampling, we use an adaptive step-size Runge–Kutta (RK) 4(5) solver [23, 65] for the Probability Flow ODE (Eq. (2)), with $\sigma(t) = t$. To embed points in the latent space of the diffusion model, we run the solver from $\sigma_{\text{min}}=0.002$. to $\sigma_{\text{max}}=80$. On the other hand, for usual sampling (decoding), we run the solver (or sampler) from $\sigma_{\text{max}}=80$ to $\sigma_{\text{min}}=0.002$.

To synthesize regular diffusion model samples, as visualized in Fig. 2, we apply the Euler–Maruyama method [66] to the sum of the Probability Flow ODE and a *Langevin diffusion* SDE [23, 39]

$$d\mathbf{x} = \underbrace{-\dot{\sigma}(t)\sigma(t)\nabla_{\mathbf{x}} \log p(\mathbf{x};\sigma(t)) dt}_{\text{Probability Flow ODE; see Eq. (2)}} - \underbrace{\beta(t)\sigma^2(t)\nabla_{\mathbf{x}} \log p(\mathbf{x};\sigma(t)) dt + \sqrt{2\beta(t)}\sigma(t) d\omega_t}_{\text{Langevin diffusion component}}, \quad (5)$$

where $d\omega_t$ is the standard Wiener process, $\beta(t) = \dot{\sigma}(t)/\sigma(t)$, and $\sigma(t) = t$. We use the sampling schedule proposed in Karras et al. [39]; in particular:

$$\sigma_i = \left(\sigma_{\text{max}}^{1/\rho} + \frac{i}{M-1} (\sigma_{\text{min}}^{1/\rho} - \sigma_{\text{max}}^{1/\rho}) \right)^\rho, \quad i \in \{0, \dots, M-1\}, \quad (6)$$

with $\rho=7.0$. We set the number of function evaluations to $M=1,000$.

Langevin Dynamics. In Sec. 3.4, we run regular Langevin dynamics:

$$\hat{\mathbf{z}}_{n+1} = \hat{\mathbf{z}}_n - \frac{\hat{\mathbf{z}}_n}{2} \Delta t + \sqrt{\Delta t} \mathcal{N}(\mathbf{0}, \mathbf{I}), \quad (7)$$

using step size $\Delta t = 0.1$. The sequence $\{\hat{\mathbf{z}}_n\}$ is then decoded using the RK solver (see above).

Latent Interpolations. For latent interpolations, we first encode points into the latent space of the diffusion model using the RK solver. We then perform linear interpolation in the diffusion model’s latent space. Subsequently, these points are decoded using the RK solver. We generally interpolate using 100 equidistant steps.

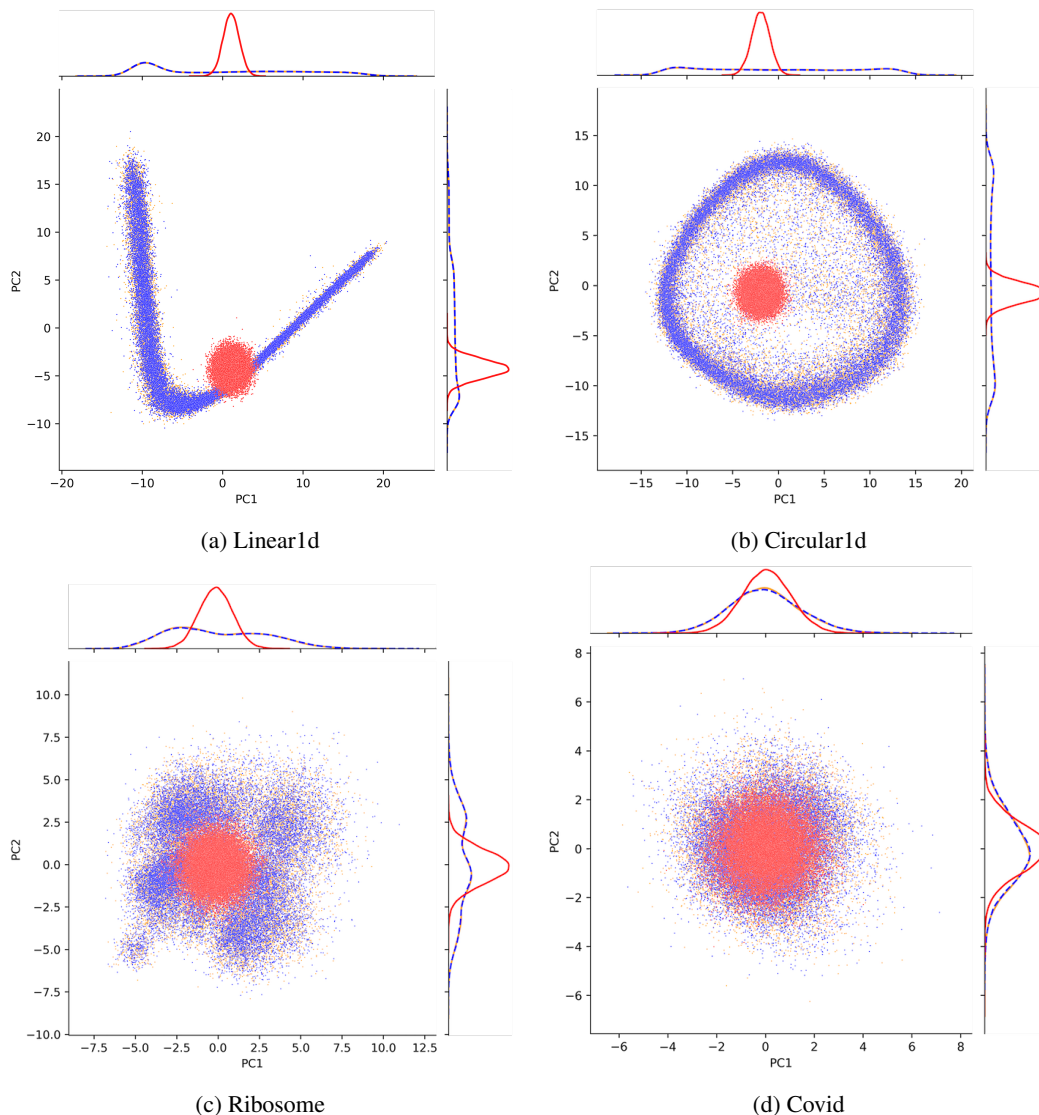


Figure 7: Marginal distributions by projecting samples along the first two principal components of the latent embeddings. Latent embeddings of the data are shown in blue; sampled latent variables from the diffusion model prior or VAE prior are shown in orange or red, respectively. Note that the data marginals are plotted with a (blue) dashed line, which ends up lying directly on top of the orange curves for the diffusion model samples. From these plots we can observe that the marginal distributions for samples from the diffusion model priors are consistent with those of the data’s latent embeddings.

A.2 Additional Plots

In Fig. 7, we show 1-dimensional marginal distributions of the principal components for all datasets in addition to the samples themselves.

In Fig. 8, we show a conformational state interpolation for *circular1d*. Leveraging the diffusion model prior, we see that the interpolation proceeds along the data manifold.

In Fig. 9, we show fast Langevin dynamics sampling leveraging the diffusion model prior for all four datasets.

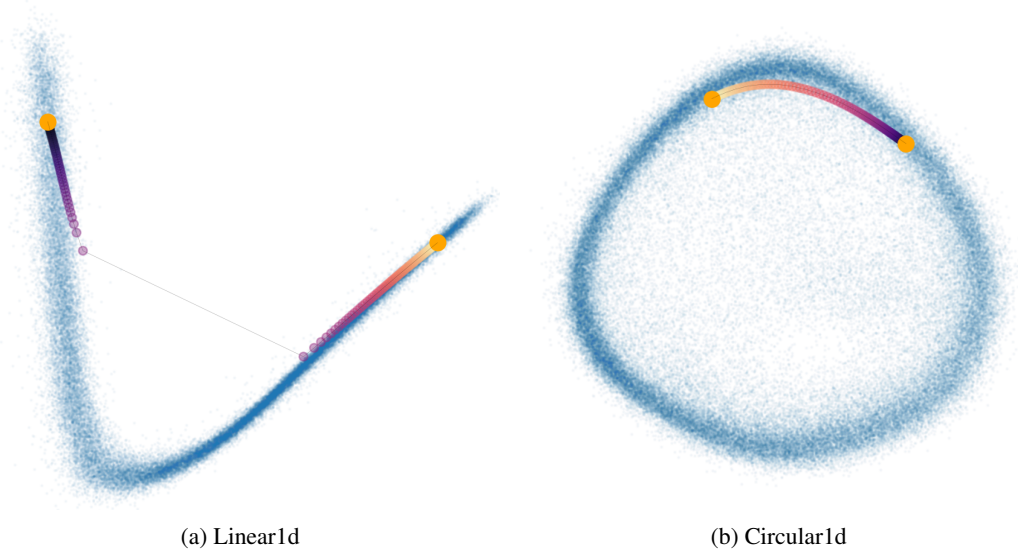


Figure 8: Latent interpolation in the diffusion model prior visualized using PCA (as in fig. 7); data latent embeddings are shown in blue. Starting and end points are shown in orange. Zoom in for details.

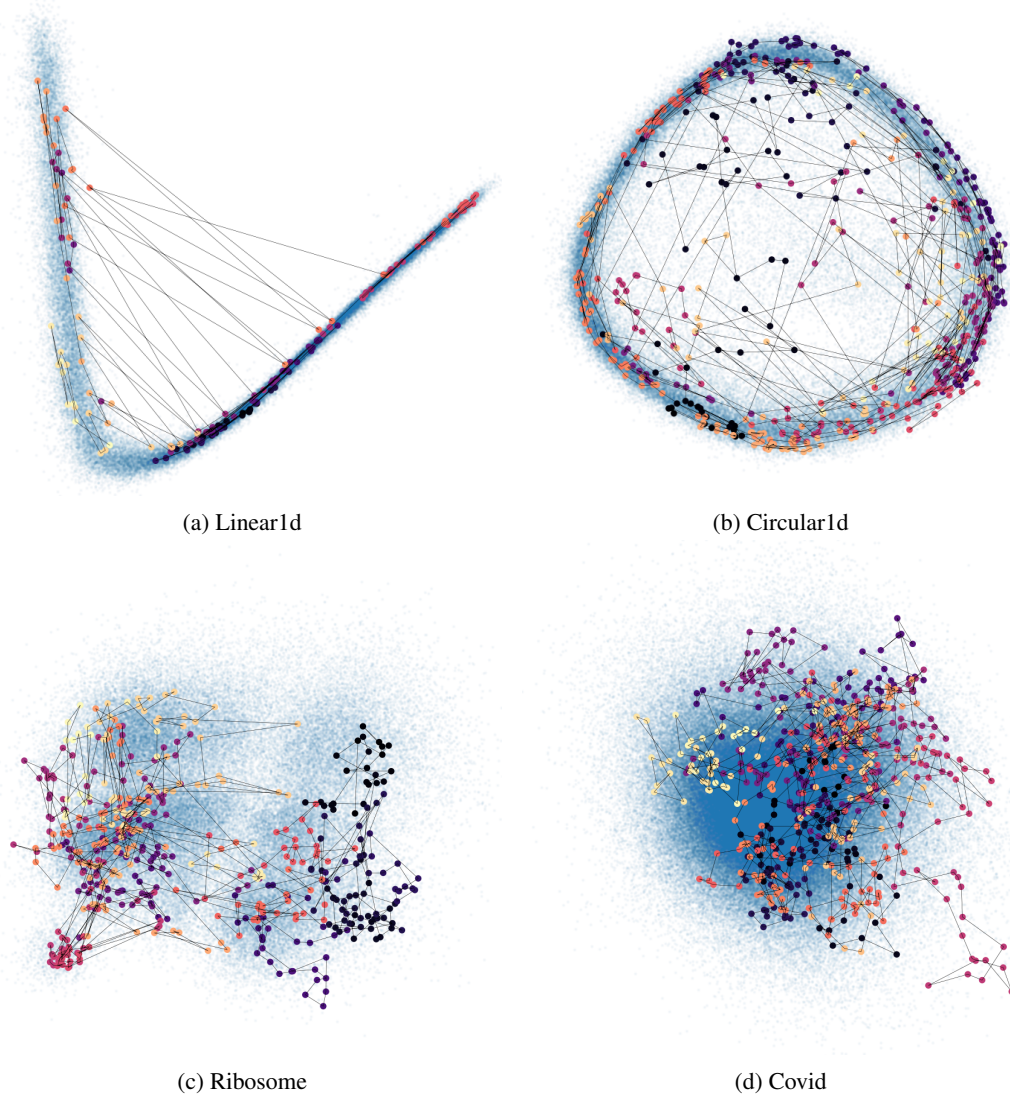


Figure 9: Langevin dynamics in the diffusion model prior visualized using PCA (as in Fig. 7). Data latent embeddings are shown in blue. The color-coding indicates the sampling path—color changes smoothly as the Langevin dynamics proceed. Zoom in for details.